Publishing Excellence Inspiring Progress
ARISTON PUBLICATIONS
Quantum Advances
ISSN: 3143-0724 www.aristonpubs.com/journal/quantum-advances https://doi.org/10.69626/qa.2025.0049

RESEARCH ARTICLE

Structural and Electronic Properties of $NaGeBr_3$ Halide Perovskite

K. Benabdelmalek[1], M. Chnafi[2], M. Hbibi[2*], S. Chouef[2], L. Belamkadem[2], M. El Hadi[2], R. Boussetta[1], O. El Abouti[1], O. Mommadi[3], A. El Moussaouy[2,4]

ABSTRACT: We present a comprehensive first-principles investigation of the structural and electronic properties of cubic $NaGeBr_3$, a lead-free germanium-based halide perovskite with promising potential for optoelectronic applications. Calculations were performed within the framework of Density Functional Theory, employing both the Generalized Gradient Approximation (GGA-PBE) and the Local Density Approximation as implemented in the Quantum ESPRESSO simulation package. Structural optimization confirms that $NaGeBr_3$ adopts a stable cubic perovskite phase with a GGA-derived equilibrium lattice parameter of 5.445 Å, in good agreement with previous theoretical studies. The bulk modulus of 22.9 GPa indicates a mechanically soft and flexible material, favorable for thin-film device integration. Electronic band structure calculations reveal a direct bandgap of approximately 0.34 eV at the high-symmetry R-point, confirming efficient light absorption and carrier generation potential. Analysis of the total and partial density of states shows that the valence band is predominantly composed of Br-4p orbitals, while the conduction band is mainly governed by Ge-4s and Ge-4p states, with negligible contribution from Na. The absence of mid-gap defect states further reinforces the material's quality and stability. These results establish $NaGeBr_3$ as a highly promising, environmentally benign candidate for next-generation solar cells and light-emitting diodes.

Keywords: $NaGeBr_3$; Halide perovskites; Density Functional Theory; Band structure; Lead-free materials; Electronic properties.

Received: 14 October 2025; Revised: 19 November 2025; Accepted: 29 November 2025; Published Online: 14 December 2025

1. INTRODUCTION

The global transition toward sustainable and efficient energy technologies has intensified the search for advanced semiconductor materials capable of replacing conventional silicon and toxic lead - based compounds in photovoltaic and optoelectronic devices. Halide perovskites, defined by the general formula ABX_3, have emerged as a remarkable class of materials owing to their tunable bandgaps, high charge carrier mobilities, long diffusion lengths, and straightforward low-temperature solution processing [1, 2]. Despite their outstanding photovoltaic performance, lead-based perovskites such as $MAPbI_3$ raise significant environmental and health concerns due to the toxicity and high-water solubility of lead [3]. This has driven extensive research into lead-free alternatives. Among the viable non-toxic substitutes, germanium (Ge)-based halide perovskites have attracted considerable attention. Germanium shares the same group-IV classification as lead but is far less toxic and more environmentally compatible [4]. Unlike tin-based analogues, which suffer from rapid oxidation of Sn^{2+} to Sn^{4+} under ambient conditions, Ge-based perovskites demonstrate comparatively better chemical stability, making them more suitable

[1] LRDSI, Department of Physics, Al-Hoceima Faculty of Science and Technology, Abdelmalek Essaâdi University, Tétouan, Morocco.
[2] OAPM group, Laboratory of Materials, Waves, Energy and Environment, Department of Physics, Faculty of Sciences, University Mohamed I, 60000 Oujda, Morocco.
[3] Research Laboratory in Sciences and Techniques, ESEFA, Ibnou Zohr University, Agadir, Morocco.
[4] Laboratory of Innovation in Science, Technology and Education, Regional Centre for the Professions of Education and Training, 60000 Oujda, Morocco.

[*] Author to whom correspondence should be addressed: mailto:drhbibi.mohammed@gmail.com (M. Hbibi)

© Ariston Publications 2025. All rights reserved.

for device integration [5]. In particular, the $NaGeX_3$ (X = Cl, Br, I) family has been identified as a promising set of fully inorganic lead-free compounds with tunable electronic and optical properties achievable through halide substitution [6]. Within this family, $NaGeBr_3$ occupies an optimal intermediate position between the wide-bandgap $NaGeCl_3$ and the narrower-bandgap, less stable $NaGeI_3$ [7]. It offers a balanced combination of structural stability, favorable electronic band characteristics, and strong optical response, making it a compelling candidate for visible-light optoelectronic applications including thin-film solar cells and light-emitting diodes (LEDs) [8]. Theoretical studies based on Density Functional Theory (DFT) have proven to be powerful and reliable tools for predicting the ground-state properties of such compounds prior to experimental synthesis. While several first-principles investigations have examined related $CsGeX_3$ and $MAGeX_3$ systems, comprehensive DFT studies focused exclusively on the structural and electronic properties of $NaGeBr_3$ with detailed computational methodology remain limited [9, 10]. The present work addresses this gap by providing a thorough and methodologically rigorous investigation, including careful convergence testing, comparative evaluation of GGA and LDA functionals, and detailed analysis of band structure and density of states. This paper is organized as follows. Section 2 describes the crystal structure and the computational methodology. Section 3 presents and discusses the results for structural properties, electronic band structure, and density of states. Section 4 summarizes the conclusions and perspectives.

2. STRUCTURE AND COMPUTATIONAL DETAILS

2.1 Crystal Structure

$NaGeBr_3$ crystallizes in the cubic perovskite structure, adopting the general ABX_3 formula. The sodium (Na) cation occupies the A-site at the corner positions (0, 0, 0), germanium (Ge) sits at the body-center B-site (0.5, 0.5, 0.5), and the three bromine (Br) atoms reside at the face-centered X-sites: (0.5, 0.5, 0.0), (0.5, 0.0, 0.5), and (0.0, 0.5, 0.5). This arrangement forms a characteristic corner-sharing $GeBr_6$ octahedral network, with Na atoms filling the dodecahedral cavities created by the octahedral framework, as illustrated in Figure 1.

2.2 Computational Details

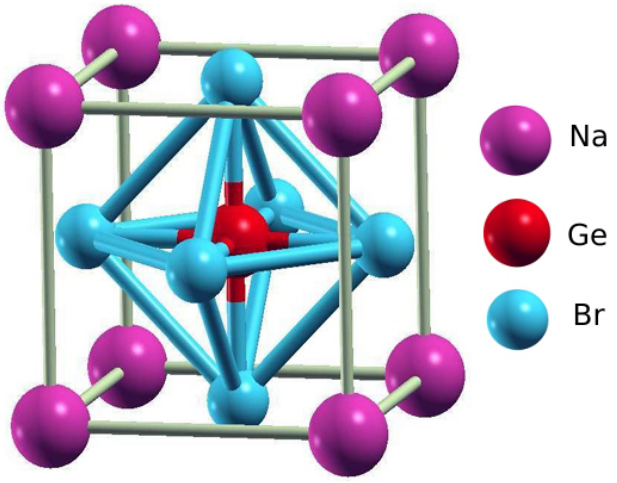

Fig. 1. Crystal structure of cubic $NaGeBr_3$. Purple spheres: Na (A-site); red sphere: Ge (B-site); cyan spheres: Br (X-site). The corner-sharing $GeBr_6$ octahedral network is clearly visible.

All first-principles calculations were performed using the Quantum ESPRESSO package [11], which implements DFT within a plane-wave basis set combined with pseudopotentials. Two exchange-correlation functionals were employed and compared: the Generalized Gradient Approximation in the Perdew-Burke-Ernzerhof (GGA-PBE) parameterization [12] and the Local Density Approximation in the Perdew-Zunger (LDA-PZ) parameterization [13]. Ultrasoft pseudopotentials (USPP) were used to describe the electron-ion interactions for all atomic species.

Prior to production calculations, systematic convergence tests were carried out to determine the optimal simulation parameters. The plane-wave kinetic energy cutoff (E_{cut}) was optimized by monitoring the variation of total energy as a function of cutoff energy from 20 to 80 Ry Figure 2(a). The total energy stabilized at 50 Ry, with negligible variation beyond this value. Similarly, the Brillouin zone sampling was tested using increasingly dense Monkhorst-Pack k-point grids Figure 2(b), and convergence was achieved at a $12 \times 12 \times 12$ mesh.

Based on these convergence tests, a kinetic energy cutoff of 60 Ry for the wavefunctions (with 480 Ry for the charge density) and a $12 \times 12 \times 12$ k-point grid was adopted for all subsequent calculations. Structural relaxation was performed using the variable-cell (vc-relax) mode with the Broyden-Fletcher-Goldfarb-Shanno (BFGS) algorithm, minimizing atomic forces below 1.0×10^{-3} Ry/Bohr and reducing the residual pressure to within 0.5 kbar. The equilibrium equation of state was extracted by fitting the total energy as a function of volume to the Murnaghan equation of state [14], yielding the lattice constant, bulk modulus, and its pressure derivative.

© Ariston Publications 2025. All rights reserved.

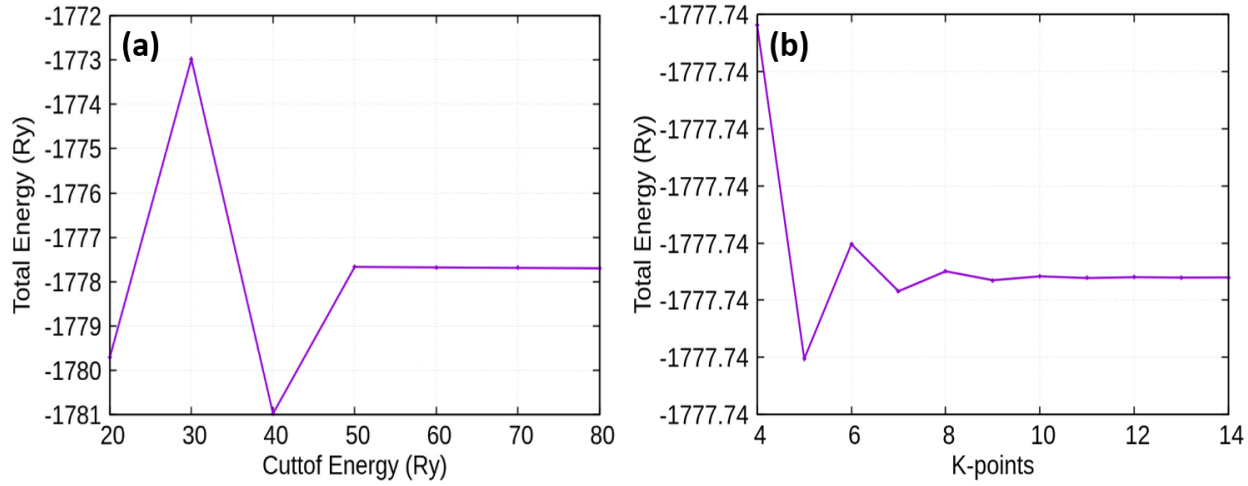

Fig. 2. Convergence of total energy with respect to (a) plane-wave cutoff energy and (b) to k-point mesh density.

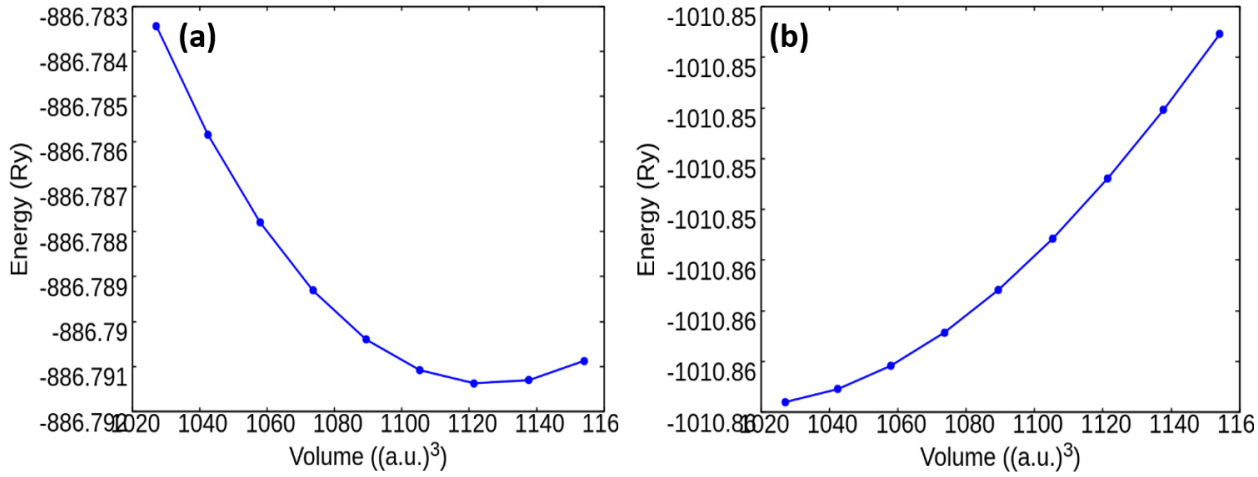

Fig. 3. Total energy as a function of volume for cubic $NaGeBr_3$ computed with GGA-PBE (a) and LDA-PZ (b) exchange-correlation functional.

3. RESULTS AND DISCUSSIONS

3.1 Structural Properties

The total energy as a function of unit cell volume was calculated using both GGA-PBE and LDA-PZ functionals and the resulting E(V) curves are shown in Figure 3(a) and 3(b), respectively. Both curves exhibit a characteristic parabolic shape with well-defined energy minima, confirming the thermodynamic stability of the cubic perovskite phase of $NaGeBr_3$. The equilibrium structural parameters extracted from Murnaghan equation of state fits are summarized in Table 1. The GGA-PBE functional predicts an equilibrium lattice constant of a_0 = 5.445 Å and an equilibrium volume of V0 = 166.89 Å³, while LDA-PZ yields a more contracted structure with a_0 = 5.316 Å and V_0 = 150.72 Å³.

This systematic underestimation of the lattice constant by LDA is well established and arises from LDA's tendency to overbind atoms by overestimating exchange-correlation effects, thereby underestimating interatomic distances [15]. The GGA result of a_0 = 5.445 Å compares favorably with the previously reported theoretical value of 5.498 Å [9], with a small deviation of approximately 0.97%, which falls within the acceptable range of DFT-GGA accuracy. The bulk modulus B_0, which quantifies the material's resistance to uniform compression, was determined to be 22.9 GPa for GGA and 29.4 GPa for LDA. These values are significantly lower than those of traditional semiconductors such as GaAs (~75 GPa) and Si (~99 GPa), indicating that $NaGeBr_3$ is a mechanically soft material. Such low bulk modulus values are characteristic of halide perovskites and are advantageous for thin-film applications where mechanical flexibility and low-temperature epitaxial

 © Ariston Publications 2025. All rights reserved.

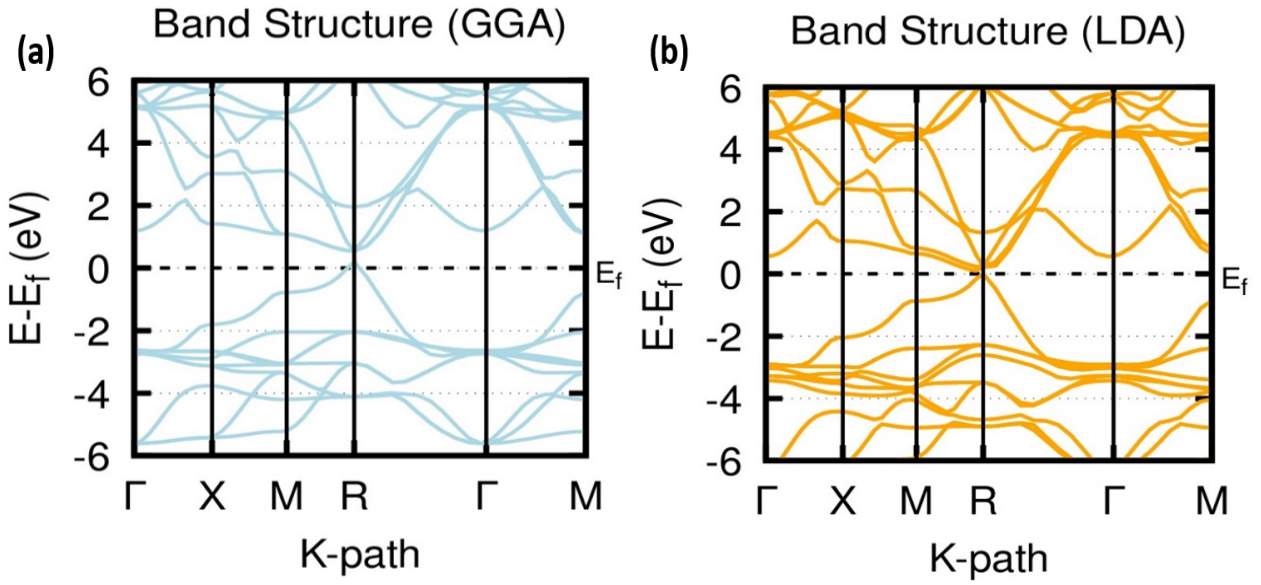

Fig. 4. Electronic band structure of cubic $NaGeBr_3$ computed along the Γ–X–M–R–Γ–M high-symmetry path using GGA-PBE (a) and LDA-PZ (b). The Fermi level (E_e) is set to 0 eV.

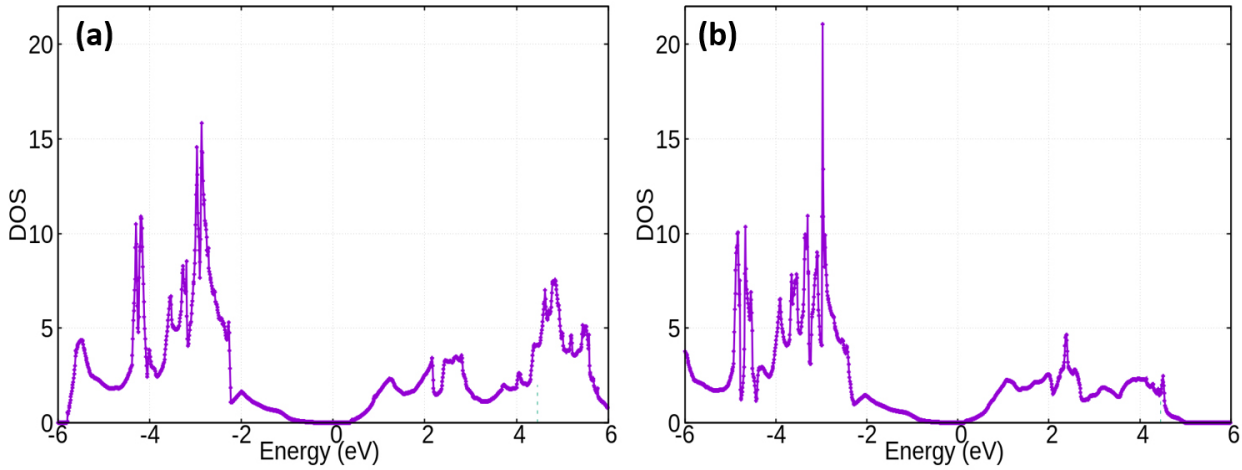

Fig. 5. Total density of states (DOS) of cubic $NaGeBr_3$ calculated with GGA-PBE (a) and LDA-PZ (b). The Fermi level is indicated by the dashed vertical line at 0 eV.

growth are desirable [16]. The pressure derivative B'_0 = 4.09 (GGA) and 4.72 (LDA) are within the typical range for halide perovskites, indicating progressive stiffening under applied pressure while maintaining moderate structural elasticity. All computed structural parameters are compiled in Table 1 alongside available literature data.

3.2 Electronic Band Structure

The electronic band structures of cubic $NaGeBr_3$ computed with GGA-PBE and LDA-PZ along the high-symmetry k-path Γ--X--M--R--Γ--M of the simple cubic Brillouin zone are presented in Figure 4. Both functionals yield a consistent qualitative picture: $NaGeBr_3$ is a direct-bandgap semiconductor, with both the valence band maximum (VBM) and the conduction band minimum (CBM) located at the same high-symmetry R-point of the Brillouin zone.

The direct bandgap energy computed with GGA-PBE is approximately 0.34 eV, while LDA-PZ gives a substantially smaller value of 0.12 eV (Table 2). The underestimation of the bandgap by LDA is a well-known artifact arising from the self-interaction error inherent in local density approximations, which causes an artificial lowering of the conduction band energy [17]. In the LDA band structure, the conduction band minimum lies unusually close to the Fermi level, which could misleadingly suggest near-metallic behavior if not interpreted carefully. The GGA-PBE result of 0.34

© Ariston Publications 2025. All rights reserved.

eV aligns more closely with previously reported theoretical values of 0.45 eV [9] and 0.78 eV [10], the remaining discrepancy being attributed to the well-known tendency of DFT-GGA to underestimate bandgaps in semiconductors due to the derivative discontinuity of the exchange-correlation functional.

The direct bandgap nature of $NaGeBr_3$ is of great significance for optoelectronic applications. In direct-gap semiconductors, optical transitions between VBM and CBM are momentum-conserving and therefore do not require phonon assistance, resulting in highly efficient radiative recombination and strong light-matter coupling. This property is essential for the design of efficient thin-film solar cells and electroluminescent devices. Furthermore, examination of the band curvature near the R-point reveals that GGA-derived bands are more strongly dispersed compared to their LDA counterparts, indicating lower effective masses for both electrons and holes, and hence higher intrinsic carrier mobilities in the GGA description.

Table 1. Calculated bandgap energies of $NaGeBr_3$ from GGA-PBE and LDA-PZ compared to theoretical values

Functional / Source	E_g (eV)	Gap Nature
GGA-PBE (this work)	0.34	Direct (R→R)
LDA-PZ (this work)	0.12	Direct (R→R)
GGA (Pingak et al. [7][9])	0.45	Direct
GGA (Saikia et al. [10][10])	0.78	Direct

3.3 Total Density of States

The total density of states (TDOS) spectra computed with both GGA-PBE and LDA-PZ functionals are displayed in Figure 5. Both calculations reveal a well-defined zero-DOS region around the Fermi level, confirming the semiconducting nature of $NaGeBr_3$ and providing an independent validation of the direct bandgap found in the band structure analysis. The width of this gap in the DOS is consistent with the bandgap values of ~0.34 eV (GGA) and ~0.12 eV (LDA) reported above.

Notably, the total DOS profiles exhibit no mid-gap impurity or defect states within the bandgap region for either functional. The absence of such in-gap states is a strong indicator of a high-quality, stoichiometrically ordered crystal structure, free from significant intrinsic defects. This is a critical advantage for optoelectronic device applications, as mid-gap states act as carrier traps and recombination centers that reduce device efficiency and increase non-radiative losses [18]. The DOS profiles further show that the valence band region (below 0 eV) contains a series of sharp peaks concentrated in the energy range from approximately -6 to 0 eV, while the conduction band DOS (above the gap) shows broader features extending beyond 2 eV. The GGA spectrum displays somewhat broader features and slightly different spectral weights compared to LDA, consistent with the different exchange-correlation treatments

3.4. Partial Density of States and Orbital Character

To identify the specific atomic orbital contributions to the electronic states, the partial (projected) density of states (PDOS) was computed using GGA-PBE and is presented in Figure 6. The PDOS analysis provides essential insight into the chemical bonding character and the nature of the electronic states near the bandgap. The PDOS clearly shows that the valence band is overwhelmingly dominated by Br-4p states, with the highest intensity concentrated in the energy region from approximately -5 to -1 eV below the Fermi level.

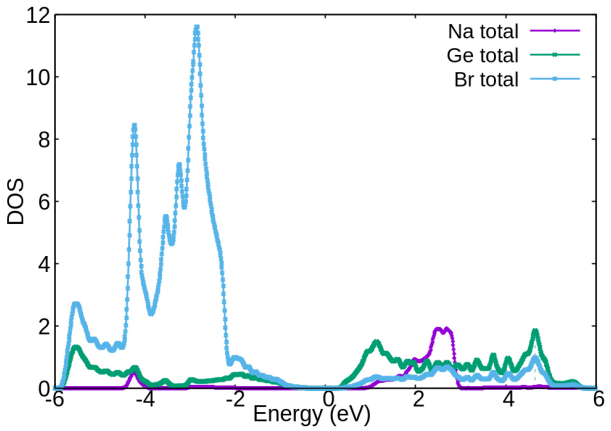

Fig. 6. Atom-projected partial density of states (PDOS) of cubic $NaGeBr_3$ computed with GGA-PBE. Contributions from Na (magenta), Ge (green), and Br (cyan) atoms are shown separately.

This behavior is entirely consistent with the role of halogen anions in halide perovskites, where the X-site halide ions provide the principal electronic states at the top of the valence band [19]. The Ge atom contributes a modest but visible density of states throughout the valence band region, primarily through its 4s and 4p orbitals, with a more pronounced contribution to the lower valence band manifold. In contrast, the Na contribution to both the valence and conduction bands is virtually negligible across the entire energy range, as expected from the fully ionic, closed-shell character of Na^+ (electronic configuration [Ne]), which does not participate directly in the frontier electronic states. The conduction band, by contrast, is mainly

© Ariston Publications 2025. All rights reserved.

composed of Ge-4s and Ge-4p states, with the Ge contribution becoming dominant above the Fermi level. This finding is consistent with the general electronic structure of Ge-based halide perovskites, where the B-site germanium cation governs the conduction band character and thus determines the roperties of photogenerated electrons [20]. The Br-4p orbitals also contribute to the lower part of the conduction band, indicating some degree of Ge-Br hybridization that gives rise to a moderate covalent bonding character at the VBM/CBM edges. This Br-4p/Ge-4s,4p orbital overlap near the band edges enhances charge delocalization and facilitates efficient carrier transport in the material. The resulting electronic structure, with a narrow direct bandgap of 0.34 eV, high DOS at the band edges, and well-separated bonding and antibonding states, collectively confirm that $NaGeBr_3$ possesses favorable intrinsic electronic properties for photovoltaic and LED applications.

4. CONCLUSION

We have performed a systematic first-principles DFT investigation of the structural and electronic properties of cubic $NaGeBr_3$ using both GGA-PBE and LDA-PZ exchange-correlation functionals within the Quantum ESPRESSO framework. Our results confirm that the material is structurally stable in the cubic phase with a lattice constant of 5.445 Å and a bulk modulus of 22.9 GPa, suggesting a mechanical flexibility ideal for thin-film applications. The electronic analysis reveals a direct bandgap of 0.34 eV at the R symmetry point and a density of states free of mid-gap defects, ensuring efficient radiative recombination and low carrier trapping. Furthermore, PDOS analysis clarifies the orbital contributions, with the valence and conduction bands dominated by Br-4p and Ge-4s/4p states, respectively. These findings establish non-toxic $NaGeBr_3$ as a compelling candidate for solar cells and LEDs, while future research employing hybrid functionals or GW corrections will be essential to refine bandgap accuracy and explore device-level optimization.

DECLARATIONS

Ethical Approval

We affirm that this manuscript is an original work, has not been previously published, and is not currently under consideration for publication in any other journal or conference proceedings. All authors have reviewed and approved the manuscript, and the order of authorship has been mutually agreed upon.

Funding

Funding Not Availbale

Availability of data and material

All of the data obtained or analyzed during this study is included in the report that was submitted.

Conflicts of Interest

The authors declare that they have no financial or personal interests that could have influenced the research and findings presented in this paper. The authors alone are responsible for the content and writing of this article.

Authors' contributions

K. Benabdelmalek, M. Hbibi: Writing - original draft, Visualization, Software, Methodology, Investigation, Data curation, Conceptualization; **M. Chnafi, S. Chouef, L. Belamkadem, M. El Hadi**: Writing - original draft, Software, Investigation, Data curation, Conceptualization; **R. Boussetta, O. Mommadi**: Writing - original draft, Software, Investigation, Data curation, Conceptualization; **O. El Abouti, A. El Moussaouy**: Writing - review & editing, Writing - original draft, Validation, Software, Methodology, Investigation, Data curation, Conceptualization.

REFERENCES

[1] Kojima, A and Teshima, K and Shirai, Y and Miyasaka, T, **2009**. Organometal halide perovskites as visible-light sensitizers for photovoltaic cells. *Journal of the American Chemical Society*, 131(17), p.6050-6051. https://doi.org/10.1021/ja809598r.

[2] Green, M A and Ho-Baillie, A and Snaith, H J, **2014**. The emergence of perovskite solar cells. *Nature Photonics*, 8(7), p.506-514. https://doi.org/10.1038/nphoton.2014.134.

[3] Ravi, V K and Mondal, B and Nawale, V V and Nag, A, **2020**. Don't let the lead out: new material chemistry approaches for sustainable lead halide perovskite solar cells. *ACS Omega*, 5(46), p.29631-29641. https://doi.org/10.1021/acsomega.0c04599.

© Ariston Publications 2025. All rights reserved.

[4] Chiara, R and Morana, M and Malavasi, L, **2021**. Germanium□based halide perovskites: materials, properties, and applications. *ChemPlusChem*, 86(6), p.879-888. https://doi.org/10.1002/cplu.202100191.

[5] Rudd, P N and Huang, J, **2019**. Metal ions in halide perovskite materials and devices. *Trends in Chemistry*, 1(4), p.394-409. https://doi.org/10.1016/j.trechm.2019.04.010.

[6] Jong, U G and Yu, C J and Ri, J S and Kim, N H and Ri, G C, **2016**. Influence of halide composition on the structural, electronic, and optical properties of mixed CH3NH3Pb(I1-xBrx)3 perovskites calculated using the virtual crystal approximation method. *Physical Review B*, 94(12), p.125139. https://doi.org/10.1103/PhysRevB.94.125139.

[7] Pingak, R K and Bouhmaidi, S and Setti, L, **2023**. Investigation of structural, electronic, elastic and optical properties of Ge-halide perovskites NaGeX3 (X= Cl, Br and I): A first-principles DFT study. *Physica B: Condensed Matter*, 663, p.415003. https://doi.org/10.1016/j.physb.2023.415003.

[8] Hasan, M N and Rifat, M N and Rony, J K and Saiduzzaman, M and Islam, M, **2025**. First-principles investigation of NaGeX3 (X= Cl, Br, I) perovskites for eco-friendly photovoltaic and optoelectronic applications. *Physics Open*, 24, p.100278. https://doi.org/10.1016/j.physo.2025.100278.

[9] Harbi, A and Bouhmaidi, S and Pingak, R K and Setti, L and Moutaabbid, M, **2023**. First-principles calculations to investigate optoelectronic, thermoelectric and elastic properties of novel lead-free halide perovskites CsRbPtX6 (X= Cl, Br and I) compounds for solar cells applications. *Physica B: Condensed Matter*, 668, p.415242. https://doi.org/10.1016/j.physb.2023.415242.

[10] Saikia, D and Alam, M and Bera, J and Betal, A and Gandi, A N and Sahu, S, **2022**. A first-principles study on ABBr3 (A= Cs, Rb, K, Na; B= Ge, Sn) halide perovskites for photovoltaic applications. *Advanced Theory and Simulations*, 5(12), p.2200511. https://doi.org/10.1002/adts.202200511.

[11] Giannozzi, P and Baroni, S and Bonini, N and Calandra, M and Car, R and Cavazzoni, C and Ceresoli, D and Chiarotti, G L and Cococcioni, M and Dabo, I and Dal Corso, A, **2009**. QUANTUM ESPRESSO: a modular and open-source software project for quantum simulations of materials. *Journal of Physics: Condensed Matter*, 21(39), p.395502. https://doi.org/10.1088/0953-8984/21/39/395502.

[12] Perdew, J P and Burke, K and Ernzerhof, M, **1996**. Generalized gradient approximation made simple. *Physical Review Letters*, 77(18), p.3865. https://doi.org/10.1103/PhysRevLett.77.3865.

[13] Perdew, J P and Zunger, A, **1981**. Self-interaction correction to density-functional approximations for many-electron systems. *Physical Review B*, 23(10), p.5048. https://doi.org/10.1103/PhysRevB.23.5048.

[14] Murnaghan, F D, **1937**. Finite deformations of an elastic solid. *American Journal of Mathematics*, 59(2), p.235-260. https://doi.org/10.2307/2371405.

[15] Absike, H and Labrim, H and Hartiti, B and Douhou, K and Ez-Zahraouy, H, **2019**. Ab initio calculations on electronic, optical, and thermoelectric properties of (Si, Pb)(co)-doped ZnS for solar cell device applications. *Journal of Physics and Chemistry of Solids*, 132, p.10-17. https://doi.org/10.1016/j.jpcs.2019.03.030.

[16] Huang, J and Chen, W, **2022**. Flexible strategy of epitaxial oxide thin films. *iScience*, 25(10), p.105041. https://doi.org/10.1016/j.isci.2022.105041.

[17] Cohen, A J and Mori-Sánchez, P and Yang, W, **2012**. Challenges for density functional theory. *Chemical Reviews*, 112(1), p.289-320. https://doi.org/10.1021/cr200107z.

[18] Guo, Z and Yuan, M and Chen, G and Liu, F and Lu, R and Yin, W J, **2024**. Understanding defects in perovskite solar cells through computation: current knowledge and future challenge. *Advanced Science*, 11(20), p.2305799. https://doi.org/10.1002/advs.202305799.

[19] Crespo, C T, **2019**. The effect of the halide anion on the optical properties of lead halide perovskites. *Solar Energy Materials and Solar Cells*, 195, p.269-273. https://doi.org/10.1016/j.solmat.2019.03.023.

[20] Bouhmaidi, S and Marjaoui, A and Talbi, A and Zanouni, M and Nouneh, K and Setti, L, **2022**. A DFT study of electronic, optical and thermoelectric properties of Ge-halide perovskites CsGeX3 (X= F, Cl and Br). *Computational Condensed Matter*, 31, p.e00663. https://doi.org/10.1016/j.cocom.2022.e00663.

 © Ariston Publications 2025. All rights reserved.